Dependence of Edge Stability on Plasma Shape and Local Pressure Gradients in the DIII-D and JT-60U Tokamaks

L.L. Lao,[1] Y. Kamada,[2] T. Oikawa,[2] L.R, Baylor,[3] K.H. Burrell,[1] V.S. Chan,[1] M. Chance,[4] M.S. Chu,[1] J.R. Ferron,[1] T. Fukuda,[2] T. Hatae,[2] A. Isayama,[2] G.J. Jackson,[1] A.W. Leonard,[1] M.A. Makowski,[5] J. Manickam,[4] M. Murakami,[3] M. Okabayashi,[4] T.H. Osborne,[1] P.B. Snyder,[1] E.J. Strait,[1] S. Takeji,[2] T. Takizuka,[2] T.S.Taylor,[1] A.D. Turnbull,[1] K. Tsuchiya,[2] M.R. Wade[3]

[1]General Atomics, P.O. Box 85608, San Diego, California 92186-5608, USA
   e-mail: lao@fusion.gat.com
[2]Japan Atomic Energy Agency, Naka-machi, Naka-gun, Ibaraki-ken, Japan
[3]Oak Ridge National Laboratory, Oak Ridge, Tennessee 37831, USA
[4]Princeton Plasma Physics Laboratory, Princeton, New Jersey 08543, USA
[5]Lawrence Livermore National Laboratory, Livermore, California 94550, USA

Abstract. The dependence of edge stability on plasma shape and local pressure gradients, P', in the DIII–D and JT–60U tokamaks is studied. The stronger plasma shaping in DIII-D allows the edge region of DIII-D discharges with Type I ("giant") ELMs to have access to the second region of stability for ideal ballooning modes and larger edge P' than JT-60U Type I ELM discharges. These JT-60U discharges are near the ballooning mode first regime stability limit. DIII–D results support an ideal stability based working model of Type I ELMs as low to intermediate toroidal mode number, n, MHD modes. Results from stability analysis of JT-60U Type I ELM discharges indicate that predictions from this model are also consistent with JT–60U edge stability observations.

1. Introduction and Overview

Two of the major issues in the design of future tokamak devices are the predictability of the edge pedestal height and control of the divertor heat load in H-mode discharges. Both of these are strongly influenced by edge stability. In H-mode discharges, edge instabilities (ELMs) are often present, driven by the large edge pedestal pressure gradient P', which is associated with the improved edge confinement, and the corresponding large edge bootstrap current density J_{BS}, The predicted performance of future tokamak devices is sensitive to the magnitude of the edge pressure pedestal assumed in the transport simulations. An improved understanding of edge instabilities will provide a more accurate prediction of future device performance.

In this paper, the dependence of edge stability on plasma shape and local P' in the DIII-D and JT-60U tokamaks is studied. Discharge shaping provides a powerful tool to test and validate ELM models by varying the stability properties of the plasma edge. DIII-D discharges have high elongation $\kappa \geq 1.8$ and a wide range of values of δ, and squareness (ξ) is possible. JT-60U discharges have moderate $\kappa \sim 1.4$ and low to moderate $\delta < 0.55$. The stronger plasma shaping in DIII-D allows the edge region of DIII-D discharges with Type I ("giant") ELMs to have access to the second region of stability for ideal ballooning modes and larger edge P' than JT-60U Type I ELM discharges. These JT-60U discharges are near the ballooning mode first regime stability limit. Stability analyses and observations from DIII-D edge stability experiments [1,2] support an ideal stability based model of Type I ELMs as low to intermediate toroidal mode number, n, kink/ballooning modes. In this model, second stability access plays a supporting role by facilitating the buildup of the edge P' and J_{BS}, which then drives lower n MHD modes [3,4]. The ELM amplitudes are assumed to be determined by the radial width of the unstable modes. Predictions from this model are consistent with many observed features of DIII-D edge stability experiments, as well as the observed increase of edge P' with δ in DIII-D and other tokamaks [4-7]. Although second ballooning stability access is a distinguishing feature of this model, it is not a necessary element of this model. With low edge

safety factor q_{95}, weak shaping, and large pedestal width, low to intermediate n kink/ballooning modes can become unstable at low edge P'.

JT-60U edge stability results provide an interesting test of this ELM model. In JT-60U discharges with moderate $\delta \sim 0.45$ and low $q_{95} \sim 3.4$, Type I ELMs are observed. The edge region of these discharges is found to have no access to the second region of stability for ideal ballooning modes. The edge P' is near the first ballooning stability limit. In discharges with similar δ but higher $q_{95} \sim 6$ obtained by increasing the toroidal magnetic field, the edge P' remains similar but the ELM amplitudes are strongly reduced and the frequency is strongly increased [8,9]. The edge region of these small amplitude "grassy" ELM discharges is found to have access to the second region of stability for ideal ballooning modes. Although these JT-60U edge stability results appear to be different from those of DIII-D, results from detailed stability analysis indicate that they are consistent with the predictions from the working ELM model. Ideal stability analysis based on experimentally reconstructed as well as simulated equilibria indicates that the low $q_{95} \sim 3.4$ JT-60U discharges are marginally stable to the intermediate $n = 5-10$ modes. A small increase in P' will strongly destabilize these intermediate n modes. The high $q_{95} \sim 6$ JT-60U discharges are stable to these intermediate $n = 5-10$ modes. This suggests that in the high $q_{95} \sim 6.0$ case the unstable modes may have $n > 10$. Modes with higher n are expected to be more localized due to shorter wavelength and will perturb a smaller edge region.

In Section 2, edge stability in DIII-D is discussed. The ideal stability based Type I ELM model as low to intermediate n MHD modes is introduced. Edge stability in JT-60U is discussed in Section 3. Finally, a discussion and a summary are given in Section 4.

2. Edge Stability in DIII-D

Stability analyses and DIII-D edge stability experimental results [1,2], particularly those from the DIII-D experiments varying the squareness parameter, suggest an ideal stability based working model of Type I ELMs as low to intermediate n kink/ballooning modes [3,4]. In this model, the main driving forces for the instability are the edge P' and the edge current density, which interact through the edge bootstrap current density J_{BS} and its effects on the second ballooning stability access. The ELM amplitudes are assumed to be determined by the radial width of the unstable mode. This is illustrated in Fig. 1, where a schematic drawing of the stability boundaries in the H-mode pedestal region for three different DIII-D discharge shapes with moderate to high squareness are shown in (P'_{edge}, n) space [4]. When the discharge shape has high squareness, the edge region has no second ballooning stability access and the critical P'_{edge} is set by the first ballooning stability limit for the highest n not stabilized by finite Larmor radius (FLR) effects. As squareness is reduced, the higher n modes become second stable and the critical P'_{edge} is set by the highest n mode without second ballooning stability access, as indicated schematically in the diagram. The amplitude of the unstable mode also increase as squareness is reduced. This is due to both the increase of P'_{edge} and an increase in the radial width of the mode at smaller n. Thus, as squareness is reduced, ELM amplitudes are expected to increase as observed experimentally.
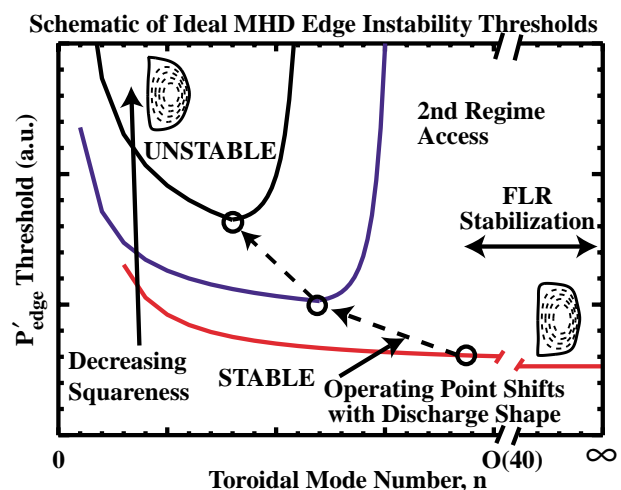

Fig. 1. A schematic drawing of the stability boundaries in the H-mode pedestal region for 3 different discharge shapes with moderate to high squareness.

The low/intermediate $n \leq 10$ branch of this diagram can be quantitatively evaluated using the ideal stability code GATO

[10], although it is computationally expensive. This is illustrated in Fig. 2 for a moderate squareness DIII-D discharge with Type I ELMs, where the critical P'_{edge} for instability is shown as a function of $n = 1$-10 computed using model equilibria based on the experimental discharge [4]. As shown in the figure, for this configuration the critical P'_{edge} is set by modes with the highest n without second ballooning stability access. The perturbation pattern and the radial structure of the unstable $n = 10$ mode are given in Fig. 3. As shown in the figure, the mode has a large peeling component localized in the edge region $\psi_N \sim 0.8$-1.0. Here ψ_N is the normalized enclosed poloidal flux. This high resolution grid point requirement makes the stability analysis of these edge modes computationally very expensive. A typical analysis of a $n = 10$ mode with 400 x 800 radial and poloidal grid points can consume more than 100 hours of CPU time on a 300 MHz Cray SV1 computer. A new ballooning representation has been implemented into GATO to reduce the poloidal grid point requirement. Initial results indicate that with this representation the number of poloidal grid points required to properly identify an unstable mode can be reduced [11].

One of the distinguishing features of this working ELM model is the second ballooning stability access in the edge region for the high n modes. This is illustrated in Fig. 4(a) for a moderate squareness DIII-D discharge. The edge pressure P and J_{BS} from transport analysis are shown in Fig. 4(b). As shown in the next section, although edge second ballooning stability access is needed to allow buildup of P'_{edge}, it is not a necessary element of this model. With low edge safety factor q_{95} and weak shaping, the low to intermediate n kink/ballooning modes can still become unstable at low edge P'. These high n ballooning modes are evaluated using the BALOO code [12]. The ballooning and peeling mode stability codes BALMSC, and ELITE are being improved to allow a more quantitative evaluation of the intermediate $10 \leq n \leq 40$ branch of the stability diagram shown in Fig. 1 [13].

3. Edge Stability in JT-60U

Recent JT-60U studies focus on the effects of triangularity δ and edge safety factor q_{95} on the ELM character. Large amplitude, low frequency ELMs (~100 Hz) are found to
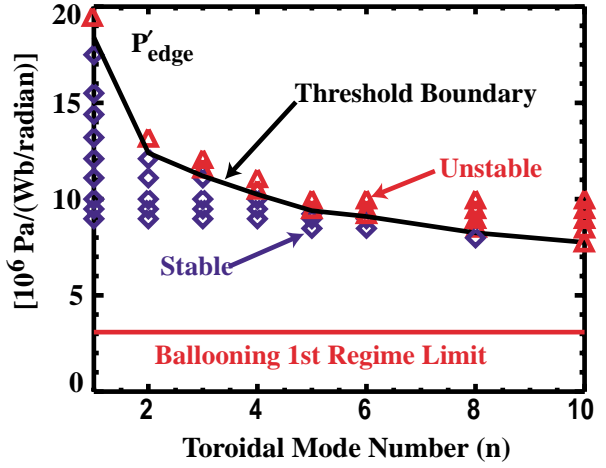
Fig. 2. Critical edge pressure gradient P'_{edge} for instability as a function of n computed using model equilibria based on a moderate squareness DIII-D discharge.
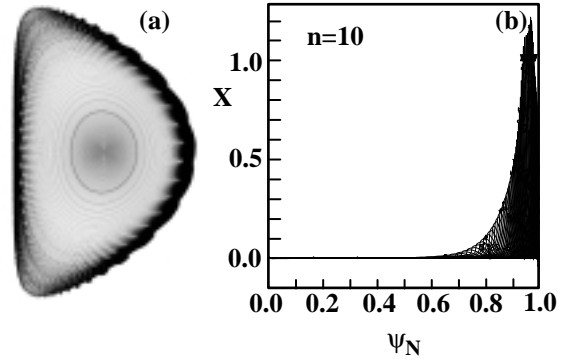
Fig. 3. (a) Perturbation pattern and (b) radial structure of an unstable n = 10 mode for a moderate squareness DIII-D discharge.
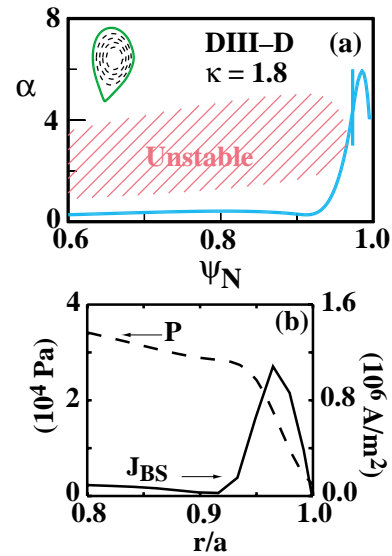
Fig. 4. (a) Ballooning stability boundary for a DIII-D moderate squareness discharge with $q_{95} \sim 3.4$, (b) Edge pressure and bootstrap current density.

disappear and small, high frequency "grassy" ELMs (~500-1000 Hz) to appear at sufficiently large $\delta \geq 0.45$, $q_{95} \geq 5$, and β_P [8,9]. At intermediate δ and lower q_{95}, the discharges are observed to consist of mixtures of giant and grassy ELMs. This is illustrated in Fig. 5.
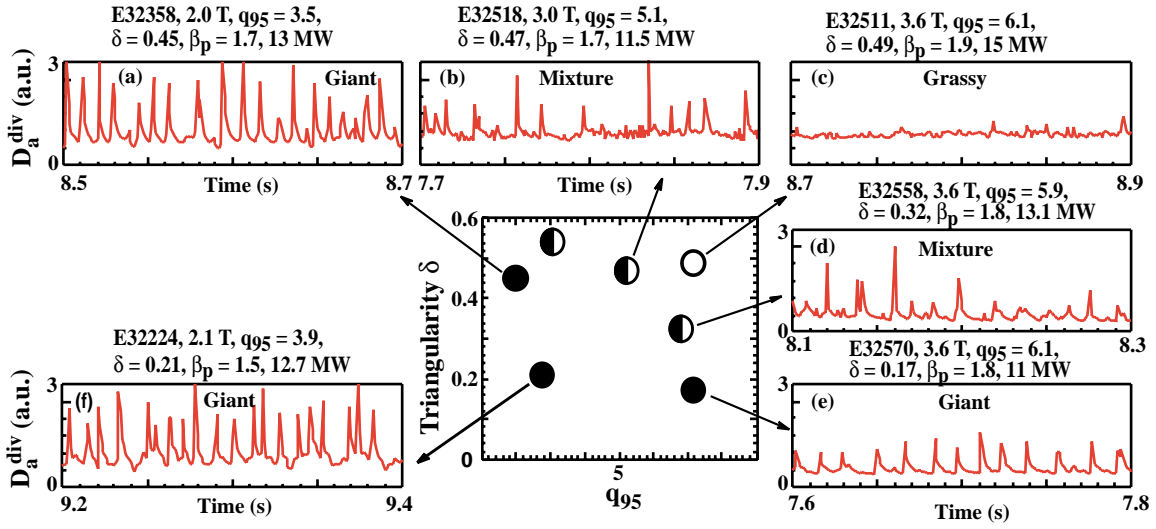

Fig. 5. Change of ELM character with δ, q_{95}, and β_P for a series of JT-60U discharges. Filled black circles indicate giant ELM discharges, open circles indicate small amplitude "grassy" ELM discharges, half-filled circles indicate discharges consist of mixtures of giant and "grassy" ELMs.

Ballooning stability analysis using equilibria accurately reconstructed using the EFIT code [14] with kinetic profiles and MSE measurements shows that the edge region of the grassy ELM discharges has second stability access. On the other hand, the results indicate that the edge region of the giant ELM discharges is near the first stability limit. These are shown in Figs. 6(a) and 6(b). This is in contrast to the DIII-D results. As shown in Figs. 4(a), 6(a), and 6(b), DIII-D discharges typically have larger edge P' than JT-60U discharges. In the DIII-D discharges, the edge region has access to the second ballooning stability regime and the large edge P' strongly exceeds the first ballooning stability limit in the neighboring surfaces. However, in the JT-60U "grassy" ELM discharges, although there is second ballooning stability access in the edge region, no substantial increase in edge P' is observed.

The stability of these two JT-60U discharges against the ideal low to intermediate $n \leq 10$ modes is evaluated using the GATO code [10]. To facilitate the analysis, experimental as well as simulated equilibria based on the experimental ones but with increasing pressure are used to guide the analysis. The results indicate that the low $q_{95} \sim 3.4$ discharges are marginally stable to the $n \sim 5$-10 kink/ballooning modes. A small increase in P' can strongly destabilize these MHD modes. When the pressure is increased by 20%, an $n = 8$ unstable edge mode can be clearly identified. This is illustrated in

Fig. 6. Comparison of the ideal ballooning stability boundary for (a) a JT-60U discharge with giant Type I ELM and $q_{95} \sim 3.4$, (b) a JT-60U discharge with "grassy" ELM and $q_{95} \sim 6.0$.

Fig. 7, where the perturbation pattern and the radial structure of the unstable $n = 8$ mode are shown. The mode has a large edge component localized in the region $\psi_N \sim 0.7$-1.0. The computed growth rates for this $n = 8$ mode are given in Fig. 8 as a function of the number of radial and poloidal grid points used in the stability evaluation. Similar to the DIII-D case, the growth rate first decreases and then increases with the number of grid points indicating this mode can not be found with a coarse grid. The high $q_{95} \sim 6.0$ case shown in Fig. 6(b) is more stable than
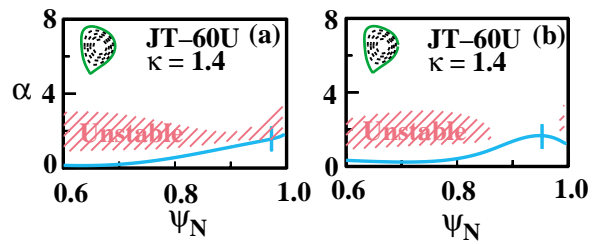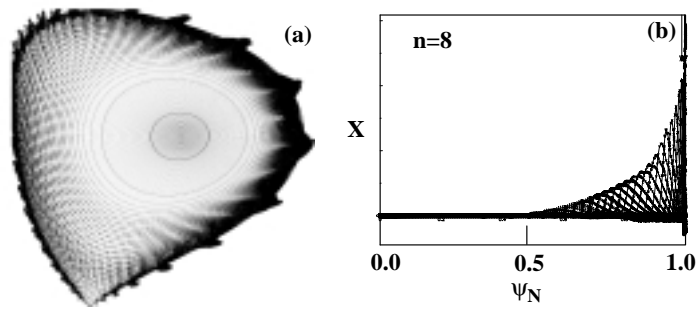
Fig. 7. (a) Perturbation pattern and (b) radial structure of an unstable n = 8 mode for a JT-60U discharge with giant Type I ELM and $q_{95} \sim 3.4$.
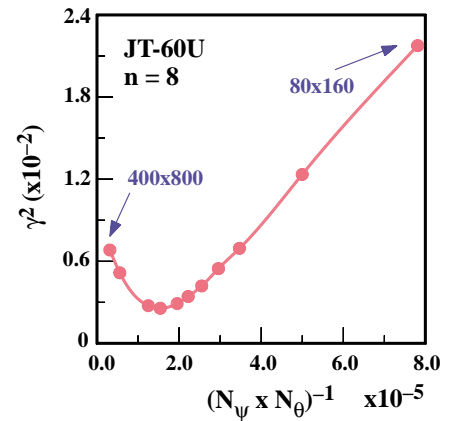

Fig. 8. Computed growth rate for an unstable n = 8 mode as a function of the number of radial and poloidal grid points used in the stability analysis for a JT-60U discharge with giant Type I ELM and $q_{95} \sim 3.4$.

the low $q_{95} \sim 3.4$ case. Even with a 20% increase in pressure, these $n \sim 5\text{-}10$ edge modes are still stable. This suggests that in the high $q_{95} \sim 6.0$ case the unstable modes may have $n > 10$. Modes with higher n are expected to be more localized due to shorter wavelength and will perturb a smaller edge region.

4. Summary

DIII-D results support an ideal stability based working model of Type I ELMs as low to intermediate toroidal mode number, n, MHD modes. Although more works need to be done to further test and validate this ELM model, initial results from stability analysis of JT-60U Type I and "grassy" ELM discharges are in support of this model.

References

[1]   LAO, L.L., et al., Nucl. Fusion **39**, 1785 (1999).
[2]   FERRON, J.R., et al., Nucl. Fusion **40**, 1411 (2000).
[3]   LAO, L.L., Plasma Phys. Control. Fusion **42**, A51 (2000).
[4]   FERRON, J.R., et al., Phys. Plasmas **7**, 1976 (2000).
[5]   OSBORNE, T.H., et al., Plasma Phys. Control. Fusion **42**, A175 (2000).
[6]   KAMADA, Y., et al., Plasma Phys. Control. Fusion **38**, 1387 (1996).
[7]   WOLF, R.C., et al., Plasma Phys. Control. Fusion **41**, 93 (1999).
[8]   KAMADA, Y., et al., Plasma Phys. Control. Fusion **42**, A247 (2000).
[9]   OIKAWA, T., et al., Bull. Am. Phys. Soc. **44**, 258 (1999).
[10] BERNARD, L.C., et al., Comput. Phys. Commun. **24**, 377 (1981).
[11] CHU, M.S., et al., Bull. Am. Phys. Soc. **44**, 79 (1999).
[12] MILLER, R.L., et al., Phys. Plasmas **4**, 1062 (1997).
[13] SNYDER, P.B., et al., in Controlled Fusion and Plasma Physics (Proc. 27th Euro. Conf. Budapest, Hungary, 2000).
[14] LAO, L.L., et al., Nucl. Fusion **30**, 1035 (1990).